

# *JHK* Observations of Faint Standard Stars in the Mauna Kea Near-Infrared Photometric System

S. K. Leggett<sup>1,2\*</sup>, M. J. Currie<sup>2,3</sup>, W. P. Varricatt<sup>4</sup>, T. G. Hawarden<sup>2,5</sup>,  
A. J. Adamson<sup>4</sup>, J. Buckle<sup>2,5</sup>, T. Carroll<sup>4</sup>, J. K. Davies<sup>2,5</sup>, C. J. Davis<sup>4</sup>,  
T. H. Kerr<sup>4</sup>, O. P. Kuhn<sup>2,7</sup>, M. S. Seigar<sup>2,8</sup>, T. Wold<sup>4</sup>.

<sup>1</sup> Gemini Observatory, 670 N. A’ohoku Place, Hilo HI 96720, USA; previously Joint Astronomy Centre

<sup>2</sup> Previously affiliated with the Joint Astronomy Centre, 660 N. A’ohoku Place, Hilo HI 96720, USA

<sup>3</sup> Rutherford Appleton Laboratory, Didcot, Oxfordshire OX11 0QX, UK

<sup>4</sup> Joint Astronomy Centre, 660 N. A’ohoku Place, Hilo HI 96720, USA

<sup>5</sup> Astronomy Technology Centre, Blackford Hill, Edinburgh EH9 3HJ, UK

<sup>6</sup> Cavendish Laboratory, Madingley Road, Cambridge CB3 0HE, UK

<sup>7</sup> LBT Observatory, University of Arizona, 933 N Cherry Ave, Tucson, AZ 85721, USA

<sup>8</sup> Department of Physics & Astronomy, University of California, Irvine, CA 92697-4575, USA

August 14th 2006

## ABSTRACT

*JHK* photometry in the Mauna Kea Observatory (MKO) near-infrared system is presented for 115 stars. Of these stars, 79 are UK Infrared Telescope (UKIRT) standards from Hawarden et al., and 42 are Las Campanas Observatory (LCO, or NICMOS) standards from Persson et al. The average brightness of the sample in all three bandpasses is 11.5 magnitudes, with a range between 10 and 15. The average number of nights each star was observed is 4, and the average of the internal error of the final results is 0<sup>m</sup>011. These *JHK* data agree with those reported by other groups to 0<sup>m</sup>02, for stars in common, which is consistent with the uncertainties. The measurements are used to derive colour transformations between the MKO *JHK* photometric system and the UKIRT, LCO and Two Micron All-Sky Survey (2MASS) systems. The 2MASS–MKO data scatter by 0<sup>m</sup>05 for redder stars, which is consistent with a dependence on stellar luminosity: the 2MASS *J* bandpass includes H<sub>2</sub>O features in dwarfs and the MKO *K* bandpass includes CO features in giants. We stress that colour transformations derived for stars whose spectra contain only weak features cannot give accurate transformations for objects with strong absorption features within one, but not both, of the filter bandpasses. We find evidence of systematic effects at the 0<sup>m</sup>02 level in the photometry of stars with  $J < 11$  and  $H, K < 10.5$  presented here and in Hawarden et al.. This is due to an underestimate of the linearity correction for stars observed with the shortest exposure times; very accurate photometry of stars approaching the saturation limits of infrared detectors which are operated in double-read mode is difficult to obtain. There are indications that four stars in the sample, GSPC S705-D, FS 116 (B216-b7), FS 144 (Ser-EC84) and FS 32 (Feige 108), may be variable. There are 84 stars in the sample presented here that have  $11 < J < 15$  and  $10.5 < H, K < 15$ , are not suspected to be variable, and have magnitudes with an estimated error  $\leq 0^m027$ ; 79 of these have an error of  $\leq 0^m020$ . These represent the first published high-accuracy *JHK* stellar photometry in the MKO near-infrared photometric system; we recommend these objects be employed as primary standards for that system.

**Key words:** infrared:stars – instrumentation: photometers – techniques: photometric – methods: observational.

## 1 INTRODUCTION

In the 1990's infrared astronomy changed radically when array cameras started to replace single-channel photometers. Not only did the field of view and spatial resolution increase markedly, but much fainter limits could be reached. One repercussion was that the existing photometric standards were too bright for the new detectors, and many groups published lists of fainter standards. These included: Bouchet et al. (1991); Casali & Hawarden (1992); Hunt et al. (1998); Persson et al. (1998); Hawarden et al. (2001); Guetter et al. (2003).

Towards the end of the 1990's and extending into this decade, modern infrared sky surveys have come on line. To maximise the output from the surveys requires a well-understood photometric system and a large grid of standard stars. Calibration of the Two Micron All Sky Survey (2MASS) is described in Cohen et al. (2003) and of the Deep Near-Infrared Survey (DENIS) in Fouqué et al. (2000). Even deeper surveys have now started at the United Kingdom Infrared Telescope (UKIRT, the UKIRT Infrared Deep Sky Survey or UKIDSS, see Hewett et al. (2006)), and at the Canada France Hawaii Telescope (CFHT, their WIRCAM instrument, Puget et al. (2004)).

Another area of recent improvement is photometry at longer infrared wavelengths. The UKIRT group presented 4-5 $\mu$ m  $L'M'$  standards in Leggett et al. (2003). Also, Cohen and collaborators have produced a series of papers extending absolute flux calibrations from the near-infrared to the mid-infrared, with particular application to mid-infrared satellites. The first paper and the most recent paper in this series, respectively, are Cohen et al. (1992) and Price et al. (2004). Calibration of the recently launched *Spitzer* infrared space telescope is described by Reach et al. (2005).

Despite this progress, a fundamental problem remained for infrared astronomers – there was no single filter set or photometric system. Not only did this mean that it was difficult to compare data, but existing filters tended to be too broad and include poor regions of the atmosphere, leading to additional noise and thus lower-accuracy data. This situation was resolved when A. Tokunaga formed a consortium to purchase a set of well-defined filters that better matched the atmospheric windows (Simons & Tokunaga 2002; Tokunaga, Simons & Vacca 2002; Tokunaga & Vacca 2005). These filters have now been widely adopted; as well as UKIRT (and UKIDSS) the following facilities have purchased Mauna Kea Observatory (MKO) near-infrared filter sets: Arizona, Boston, Cornell, Florida, Hawaii, Kyoto, Montreal, Ohio State, Tohoku, Tokyo, Virginia and Wyoming Universities; the Anglo-Australian Observatory, CalTech, Center for Astrophysics, CFHT, European Southern Observatory, Gemini, Grenoble Observatory, the NASA Infrared Telescope Facility, the Isaac Newton Group, Keck, Korea Observatory, National Astronomical Observatory of Japan, National Optical Astronomy Observatory, Nordic Optical Telescope, Osservatorio Astrofisico di Arcetri, Rome Observatory, and Telescopio Nazionale Galileo.

In this paper we present a set of standard stars observed at UKIRT using the UKIRT Fast Track Imager (UFTI) and *JHK* filters in the MKO system. The sample is described in §2, the photometric system in §3, the observing and analysis techniques in §4 and the results are given in §5. Comparison

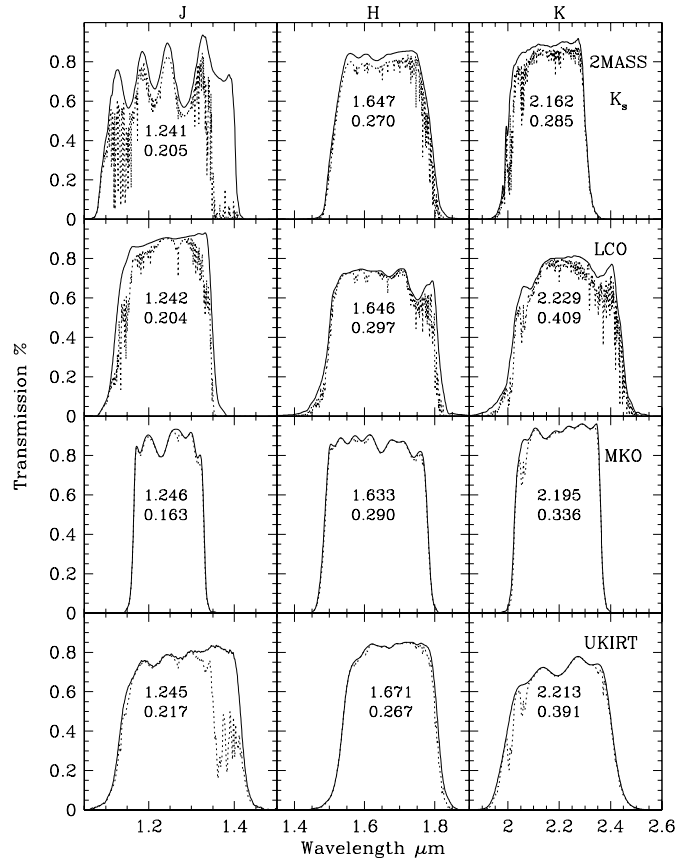


**Figure 1.** *JHK* filter transmission profiles, where the dotted line includes typical site-dependent atmospheric effects. Central wavelengths and half-power bandwidths are indicated for filter+atmosphere profiles. See Tokunaga & Vacca (2005) for a discussion of isophotal and effective wavelengths for the MKO filter set.

to published observations of the sample are given in §6. Our conclusions are given in §7.

## 2 THE SAMPLE

The sample consists primarily of UKIRT Faint Standards (Hawarden et al. 2001) and Las Campanas (LCO, or NICMOS) standards (Persson et al. 1998). Two stars from Hawarden et al., FS 18 and 118, have been removed from this sample due to the presence of a nearby star that makes aperture photometry less accurate. Three additional unreddened A0 stars, or stars with zero colours, were taken from Landolt (1992). Such stars are useful for extrapolating magnitudes to other bandpasses. The sample is listed in Table 1; coordinates are taken from the Simbad astronomical database, and proper motions and types from sources provided by the database. References are given in Table 1. For stars without spectral types in the literature we have estimated an approximate type from colour, where possible.

Table 1. Standard Stars.

UKIRT FS No.	Name	Coordinates (J2000)		Proper Motion (mas/yr)		P. M. Ref.	Spectral Type	Type Ref.
		RA	Dec	RA	Dec			
101	CMC 400101	0:13:43.6	+30:38:00	-5.3	-8.9	1	F0	2
...	BRI B0021-0214	0:24:24.6	-1:58:20	-136	+162	3	M9.5V	4
102	GSPC P525-E	0:24:28.4	+7:49:02	...	...	...	G3	5
1	G158-100	0:33:54.6	-12:07:59	+154	-183	6	DK-G	7
103	GSPC P241-G	0:36:29.6	+37:42:54	...	...	...	K2	5
2	SA92-342	0:55:09.9	+0:43:13	-2.2	-0.2	1	F5	8
...	GSPC S754-C	1:03:15.9	-4:20:44	...	...	...	F/G <sup>†</sup>	...
3	Feige 11	1:04:21.7	+4:13:37	+12.3	-28.6	9	sdB	10
104	GSPC P194-R	1:04:59.6	+41:06:31	+0.4	-4.3	1	A7	5
105	GSPC P527-F	1:19:08.2	+7:34:12	...	...	...	K1	5
106	GSPC P152-F	1:49:46.9	+48:37:53	...	...	...	K4	5
107	CMC 600954	1:54:10.0	+45:50:38	-25.1	-4.0	11	G0	2
5	Feige 16	1:54:34.7	-6:46:00	...	...	...	A0	7
4	SA 93-317	1:54:37.7	+0:43:00	-9.3	-18.5	1	F5	8
6	Feige 22	2:30:16.6	+5:15:51	+71.2	-24.6	9	DA3	12
...	GSPC P530-D	2:33:32.2	+6:25:38	...	...	...	G <sup>†</sup>	...
7	SA 94-242	2:57:21.2	+0:18:39	...	...	...	A2	8
108	CMC 502032	3:01:09.8	+46:58:48	+1.1	-0.7	1	F8	2
...	TVLM 832-38078	3:04:01.8	+00:45:50	...	...	...	M-V	13
109	LHS 169	3:13:24.2	+18:49:38	+1283	-1061	3	esdK7	14
...	GSPC P247-U	3:32:03.0	+37:20:41	...	...	...	G/K <sup>†</sup>	...
110	GSPC P533-d	3:41:02.4	+6:56:13	...	...	...	G5	5
111	CMC 601790	3:41:08.6	+33:09:36	+2.5	+3.0	11	G5	2
112	GSPC S618-D	3:47:40.7	-15:13:14	...	...	...	G0	5
10	GD 50	3:48:50.2	-0:58:31	...	...	...	DA1	12
113	GSPC P117-F	4:00:14.1	+53:10:39	...	...	...	K0	5
114	Melotte 25 LH 214	4:19:41.6	+16:45:22	...	...	...	M7V	15
115	B216-b5	4:23:18.2	+26:41:15	...	...	...	...	...
116	B216-b7	4:23:50.2	+26:40:07	...	...	...	...	...
117	B216-b9	4:23:56.5	+26:36:38	...	...	...	...	...
11	SA 96-83	4:52:58.9	-0:14:41	+0.3	-3.2	1	A3	8
119	HD 289907	5:02:57.5	-1:46:43	+1.3	-5.7	1	A2	2
...	GSPC S840-F	5:42:32.2	+0:09:04	...	...	...	G <sup>†</sup>	...
12	GD 71	5:52:27.6	+15:53:13	+92	-189	12	DA1	12
13	SA 97-249	5:57:07.6	+0:01:12	+19.3	+2.4	1	G5V	8
120	LHS 216	6:14:01.2	+15:09:53	+628	-1249	3	sdM2	14
...	GSPC S842-E	6:22:43.7	-0:36:30	...	...	...	G/K <sup>†</sup>	...
...	SA 98-653	6:52:05.0	-0:18:18	-0.3	-3.5	1	B9	8
121	GSPC S772-G	6:59:46.8	-4:54:33	...	...	...	K3	5
122	GSPC P161-D	7:00:52.0	+48:29:24	...	...	...	G0	5
14	Rubin 149A	7:24:14.0	-0:32:42	...	...	...	O9-B2p	7
...	Rubin 149D	7:24:15.4	-0:32:48	+0.70	-8.30	1	A0	2
...	GSPC P309-U	7:30:34.6	+29:51:12	...	...	...	G <sup>†</sup>	...
...	GSPC S495-E	8:27:12.5	-25:08:01	...	...	...	G/K <sup>†</sup>	...
...	GSPC P545-C	8:29:25.2	+5:56:08	...	...	...	F <sup>†</sup>	...
...	LHS 2026	8:32:30.5	-1:34:39	+155	-473	3	M6Ve	16
...	GSPC S705-D	8:36:12.5	-10:13:39	...	...	...	F/G <sup>†</sup>	...
15	M67-I-48	8:51:05.7	+11:43:46	...	...	...	G5IV-V	5
123	GSPC P486-R	8:51:11.8	+11:45:22	-7.7	-5.6	9	B8V	17
16	M67-IV-8	8:51:15.1	+11:49:21	...	...	...	G1V	5
17	M67-IV-2	8:51:19.7	+11:52:11	...	...	...	G4V	5
124	LHS 254	8:54:12.3	-8:05:00	+919	-789	3	M6.5V	14
125	GSPC P259-C	9:03:20.6	+34:21:04	...	...	...	G8	5
126	GSPC P487-F	9:19:18.7	+10:55:54	...	...	...	K3	5
...	GSPC S852-C	9:41:35.9	+0:33:12	...	...	...	G <sup>†</sup>	...
...	GSPC S708-D	9:48:56.5	-10:30:32	...	...	...	K <sup>†</sup>	...
127	GSPC P212-C	10:06:29.0	+41:01:27	...	...	...	F9	5
19	G 162-66	10:33:42.8	-11:41:38	-342	-27.2	18	DA2	12
...	GSPC P550-C	10:33:51.9	+4:49:05	...	...	...	F <sup>†</sup>	...
128	LHS 2347	11:05:10.5	+7:06:50	-466	-151	19	M5V	16
20	G 163-50	11:08:00.0	-5:09:26	-63	-440	3	DA3	12

**Table 1** – *continued*

UKIRT FS No.	Name	Coordinates (J2000)		Proper Motion (mas/yr)		P. M. Ref.	Spectral Type	Type Ref.
		RA	Dec	RA	Dec			
129	LHS 2397aAB	11:21:49.3	−13:13:08	−508	−80	3	M8V+L7.5	20
130	GSPC P264-F	11:24:55.9	+34:44:39	...	...	...	K4	5
21	GD 140	11:37:05.1	+29:47:58	−146.9	−5.9	9	DA3	12
131	GSPC P266-C	12:14:25.5	+35:35:55	...	...	...	F8	5
132	GSPC S860-D	12:21:39.4	−0:07:13	...	...	...	G1	5
33	GD 153	12:57:02.3	+22:01:53	−33	−206	3	DA1	12
133	GSPC P172-E	13:15:52.8	+46:06:37	...	...	...	G9	5
...	GSPC S791-C	13:17:29.6	−5:32:37	...	...	...	F/G <sup>†</sup>	...
23	M3-193	13:41:43.7	+28:29:51	+3.4	+2.0	21	G8III	5
...	GSPC P133-C	13:58:40.3	+52:06:24	...	...	...	F <sup>†</sup>	...
...	GSPC P499-E	14:07:34.0	+12:23:51	...	...	...	G <sup>†</sup>	...
134	LHS 2924	14:28:43.3	+33:10:38	−337	−747	19	M9Ve	16
135	GSPC S867-V	14:40:58.0	−0:27:48	...	...	...	G5	5
...	GSPC P272-D	14:58:33.1	+37:08:33	...	...	...	G <sup>†</sup>	...
136	GSPC S868-G	14:59:32.1	−0:06:17	...	...	...	K2	5
...	TVLM 868-53850	15:00:26.4	−0:39:28	...	...	...	M5Ve	22
...	TVLM 868-110639	15:10:17.2	−2:41:07	...	...	...	M9V	4
...	GSPC S870-T	15:39:03.6	+0:14:54	...	...	...	G <sup>†</sup>	...
...	GSPC P177-D	15:59:14.0	+47:36:42	...	...	...	G2V	23
137	GSPC P565-C	16:26:42.8	+5:52:20	...	...	...	G1	5
138	GSPC P275-A	16:28:06.7	+34:58:48	−11.7	+5.3	1	A1	5
...	GSPC P330-E	16:31:33.9	+30:08:47	...	...	...	G2V	23
139	GSPC P137-F	16:33:53.0	+54:28:22	...	...	...	K1	5
27	M13-A14	16:40:41.3	+36:21:13	+3.9	−1.8	24	G8IV/V	5
140	GSPC S587-T	17:13:22.7	−18:53:34	...	...	...	G9	5
...	GSPC P138-C	17:13:44.6	+54:33:21	...	...	...	G <sup>†</sup>	...
141	P489-D	17:48:58.9	+23:17:44	...	...	...	G2	5
35	GSC 00441-01200	18:27:13.5	+4:03:09	−9.0	−4.4	18	K0	5
143	Ser-EC68	18:29:53.9	+1:13:31	...	...	...	...	...
144	Ser-EC84	18:29:57.0	+1:12:47	...	...	...	...	...
...	GSPC P182-E	18:39:33.7	+49:05:38	...	...	...	G <sup>†</sup>	...
...	LDN 547	18:51:15.6	−4:16:02	...	...	...	...	...
146	GSPC P280-U	18:54:04.0	+37:07:19	...	...	...	K1	5
147	GSPC P230-A	19:01:55.3	+42:29:19	−1.4	−0.1	1	A0	2
...	GSPC S808-C	19:01:55.5	−4:29:12	...	...	...	G/K <sup>†</sup>	...
148	GSPC S810-A	19:41:23.4	−3:50:57	−1.5	−4.5	9	A0	25
149	GSPC P338-C	20:00:39.2	+29:58:38	+4.5	−4.3	1	B7.5V	26
150	CMC 513807	20:36:08.4	+49:38:24	+8.2	+9.3	1	G0	2
...	GSPC S813-D	20:41:05.2	−5:03:42	...	...	...	G <sup>†</sup>	...
34	EG 141	20:42:34.8	−20:04:35	+354.6	−97.9	9	DA2.5	12
...	GSPC P576-F	20:52:47.4	+6:40:05	...	...	...	G <sup>†</sup>	...
151	GSPC P340-H	21:04:14.8	+30:30:21	...	...	...	G2	5
29	G 93-48	21:52:25.4	+2:23:20	+23.0	−303.0	9	DA3	12
...	BRI B2202-1119	22:05:35.7	−11:04:29	−271	−170	3	M5.5V	4
152	GSPC P460-E	22:27:16.1	+19:16:59	...	...	...	K1	5
30	SA 114-750	22:41:44.7	+1:12:36	...	...	...	B9	8
153	S820-E	23:02:32.1	−3:58:53	...	...	...	K2	5
31	GD 246	23:12:23.1	+10:47:04	+127	−11	12	DA1	12
32	Feige 108	23:16:12.4	−1:50:35	...	...	...	sdB	27
154	GSPC S893-D	23:18:10.1	+0:32:57	...	...	...	G0	5
...	GSPC S677-D	23:23:34.5	−15:21:06	...	...	...	F <sup>†</sup>	...
...	GSPC P290-D	23:30:33.5	+38:18:57	...	...	...	G <sup>†</sup>	...
...	PG 2331+055A	23:33:44.5	+5:46:41	...	...	...	sd	10
155	CMC 516589	23:49:47.8	+34:13:05	...	...	...	K5V	28

<sup>†</sup> Spectral type estimated from  $B - V$  and  $V - K$  from Lasker et al. 1988 and this work.

References: (1) The Tycho Reference Catalogue, Hog et al. 1998 (2) AGK3 Catalogue, Heckmann & Dieckvoss 1975 (3) Salim & Gould 2003 (4) Kirkpatrick, Henry & Simons 1995 (5) Hawarden et al. 2001 (estimated from colour or colour-magnitude diagrams) (6) Harrington & Dahn 1980 (7) Turnshek et al. 1990 (8) Drilling & Landolt 1979 (9) The Hipparcos Catalogue, Perryman et al. 1997 (10) The Palomar-Green Survey, Green, Schmidt & Liebert 1986 (11) PPM North Star Catalogue, Roeser & Bastian 1988 (12) McCook & Sion 1999 (13) Tinney 1993 (14) Gizis 1997 (15) Reid & Hawley 1999 (16) Leggett 1992 (17) Pesch 1967 (18) The Second U.S. Naval Observatory CCD Astrograph Catalog (UCAC2), Zacharias et al. 2004 (19) Bakos, Sahu & Németh 2002 (20) Freed, Close & Siegler 2003 (21) Tucholke, Scholz & Brosche 1994 (22) Gizis 2002 (23) Colina & Bohlin 1997 (24) Kadla 1966 (25) Henry Draper Catalogue, Cannon & Pickering 1989 (26) Straizys & Kalytis 1981 (27) Greenstein & Sargent 1974 (28) Stephenson 1986.

### 3 PHOTOMETRIC SYSTEMS

#### 3.1 Filters

Figure 1 plots the transmission curves of the MKO consortium *JHK* filters as well as those of the UKIRT filter set (used by Hawarden et al. 2001), the set used by Persson et al. (1998: LCO) and the 2MASS filters. Colour transformations between these systems are discussed in §6.2. Profiles are shown with and without atmospheric absorption. Atmospheric transmissions appropriate for each site were taken from the sources given by Stephens & Leggett (2004). The *J* and *K* MKO filters are narrower than the other filter sets (except for 2MASS  $K_s$ ) to avoid the poor regions of the atmospheric windows. The 2MASS and UKIRT *J*-band filters are particularly prone to atmospheric absorption and therefore noise. For further discussion, see Simons & Tokunaga (2002) and Tokunaga, Simons & Vacca (2002).

#### 3.2 Optical Elements

As summarised in Hawarden et al. (2001); Leggett et al. (2003); Stephens & Leggett (2004), the commonly used near-infrared optical elements have transmission or absorption wavelength responses that are flat across the *JHK* filter bandpasses. Hence instrument and telescope optics typically do not significantly affect the photometric system. Hawarden et al. (2001) found that even changes in UKIRT's optical/infrared dichroic coating did not affect the *J* bandpass. Stephens & Leggett (2004) did find that, for the very structured spectra of late L and T dwarfs, the variations between detector quantum efficiency and anti-reflection coatings can affect measured magnitudes by up to 1%. However for stars with a more typical spectral energy distribution, such as those in this sample, these effects are negligible. Hence the results presented here are appropriate for any camera equipped with the *JHK* MKO filters and a detector with a reasonably flat sensitivity curve (such as UKIRT's Wide Field Camera WFCAM – but see further discussion in §6.2).

## 4 TECHNIQUES

#### 4.1 Observations

All observations presented here were made at UKIRT using the UKIRT Fast Track Imager, UFTI (Roche et al. 2003). UFTI contains a HAWAII-I HgCdTe detector, with  $1024 \times 1024$  0.091 arcsecond pixels. For standard star observations a  $512 \times 512$  subarray readout was used, allowing minimum exposure times of 1 second. UFTI was outfitted with MKO filters from its commissioning in 1998 October.

The data presented here were taken over 21 photometric nights between 2001 January 23 and 2004 December 29. 10 to 50 standards were observed on whole or partial nights. One to three would be repeated to measure the extinction on each night and the stars would be observed between one and ~two airmasses. Exposure times ranged from 1 second to 60 seconds, but were usually around 8 seconds at *J* and 4 seconds at *H* and *K*. On nights of very poor or very good seeing the exposure times would be adjusted to keep the peak data counts on the star between 500 and 4000 data

numbers, as far as possible. Typically a five-position jitter pattern was used with 10-arcsecond offsets. Nine-position jitters were used for stars fainter than 15th magnitude.

#### 4.2 Data Reduction

The data were reduced using the ORAC-DR pipeline (Cavanagh et al. 2003). Details of the reduction recipes (JITTER\_SELF\_FLAT\_APHOT, BRIGHT\_POINT\_SOURCE\_APHOT) are presented in the ORAC-DR Imaging Data Reduction User Guide<sup>1</sup>. ORAC-DR uses various Starlink software packages to reduce astronomical data.

The raw image counts are first corrected for non-linearity using the empirical correction determined at the observatory in 2000 October:

$$\text{true} = \text{measured} / (1 + (6.1 \cdot 10^{-6} * \text{measured}))$$

Note that the measured counts are *larger* than the corrected counts. This relationship holds for measured counts fewer than 10000 data numbers (DN) – above this limit the detector goes into hard saturation where measured counts will be much *smaller* than predicted. The non-linearity correction is small – around 2% at the typical value of 4000 counts. We discarded data where any pixel was higher than 10000 DN.

The raw images, and the engineering data used to derive the non-linearity correction, were taken in non-destructive read mode, where the detector is reset, read out, exposed and read out again, and the counts in the stored image are the difference between the two reads. The linearity correction we have applied to the images is not strictly correct, as a correction should be applied to each individual read and not the difference (Persson et al. 1998; Vacca, Cushing & Rayner 2004). However in §6.3 we show that the error is insignificant except for the brightest stars in the sample which were observed with exposure times similar to the array readout time; for these stars the effect is small but significant. Note that UFTI's non-linearity correction goes in the opposite sense to the more typical well-filling saturation behaviour, where lower, not higher, counts would be expected as signal increases. The somewhat unusual UFTI controller may be the cause of this linearity behaviour. The controller is derived from the CIRSI controller (Beckett et al. 1998) which in turn is based on an LSR-Astrocams (later PerkinElmer Life Science) 4100 CCD controller. During the read of each pixel, a fast video switch in the interface switches between the real output of the array and a dummy level, to remove drifts.

After correcting for non-linearity, each frame is bad-pixel masked, dark-subtracted and flat-fielded. Dark frames are taken with every star. Any darks that suffered from latent images are rejected. Flat fields are created from median-filtered and object-masked jittered images of the fainter standards. Object masking detects objects with 12 connected pixels at  $1 \sigma$  above the sky level. The locations, shapes, orientations and sizes are used to make a mask which is applied to the dark-subtracted frames to generate the flat field. Jittered frames of fainter stars are used to generate the flat field so that the background level is dominated by sky

<sup>1</sup> <http://www.starlink.ac.uk/star/docs/sun232.htx/sun232.html>

**Table 2.** MKO *JHK* Extinction (Magnitudes/Airmass).

Filter	Min.	Max.	Mean	Std. Devn.	Calculated for pwv:	
					1mm	4mm
<i>J</i>	0.012	0.090	0.047	0.024	0.006	0.014
<i>H</i>	0.000	0.072	0.029	0.020	0.005	0.015
<i>K</i>	0.000	0.124	0.052	0.028	0.017	0.019

noise and not read noise. For UFTI, images taken with *J* exposure times  $\geq 20$  seconds, and *H* and *K* exposure times  $\geq 5$  seconds, are background-noise-limited. For brighter standards that were not background-noise-limited, the closest-in-time flat field, generated with a faint standard, was used.

Finally, a mosaic is created from the flat-fielded jitter set of five or nine pointings. Aperture photometry is carried out on each source using a 7-arcsecond diameter aperture, with sky annuli from 10.5 to 17.5 arcseconds. This is large enough to include all the light from the star even on nights of mediocre seeing, without compromising signal-to-noise. On one night with poor seeing (20020217) an 8-arcsecond aperture had to be used.

ORAC-DR reports photometric errors on each individual flat-fielded frame, as well as on the mosaic. For this work we have conservatively adopted the uncertainty to be the standard deviation in the mean of the measurements of a jitter set. This standard deviation is 1–2%, compared to the millimag-level error calculated by ORAC-DR from the sky variance of the mosaic.

Zeropoint magnitudes are calculated for each measurement by subtracting the instrumental magnitude from the catalogue magnitude. These zeropoints are plotted against airmass for each filter for each night. A linear extinction curve is fitted to the data using the extinction star(s), and each catalogue magnitude adjusted so that the star would agree with the average zeropoint at an airmass of one, as defined by that night’s sample. In this way we revised the standard stars’ catalogue of *JHK* magnitudes after every observing run, such that the group became more self-consistent as time went on. The initial standard star catalogue consisted of UKIRT Faint Standard values transformed to the MKO system using the preliminary colour terms given in Hawarden et al. (2001).

For this paper we re-reduced the data from all 21 nights using the most recent version of the catalogue, to ensure that the entire set was handled consistently. Linear extinction curves were fitted for each night in each filter using the entire night’s data (i.e. not just the extinction stars). The scatter around this curve was 0<sup>m</sup>.02 or less. A single *J*, *H* or *K* value was calculated for each star for each night and these values then averaged over all nights. The results are given in the next section.

## 5 RESULTS

### 5.1 Extinction

Table 2 lists our measured extinction values at *JHK*, determined by linear regression to the [airmass, zeropoint] values (for airmass ranging from 1 to around 2), for the sample of

21 nights. The uncertainty in the nightly extinction value is  $\sim 0.01$  magnitudes/airmass. Water vapour measurements over these nights ranged from a 225 GHz  $\tau$  of 0.04 to 0.27 (average 0.10), corresponding to a precipitable water vapour (pwv) of between 1 and 5 mm (average 2 mm). We find no correlation between  $\tau$  and extinction, as expected for these filters which are well matched to the atmospheric windows. Tokunaga, Simons & Vacca (2002) calculate the extinction due to water vapour for the MKO filters, for 1 to 4 mm of water vapour, and these values are given in Table 2. It can be seen that the measured values are higher, which would be expected as extinction due to scattering is not included in the calculated values. Tüg, White & Lockwood (1977), for example, have shown that aerosol scattering is significant in the far red. The difference between the measured and predicted extinction values in Table 2 indicate that scattering can contribute between 0 and  $\sim 0.1$  magnitudes/airmass to the extinction at *JHK*, on the summit of Mauna Kea. For accurate photometry of targets with airmass differing significantly from their calibrators, the extinctions must be determined on each night.

### 5.2 *JHK* magnitudes

Table 3 gives our weighted mean *JHK* magnitudes, the estimated error of that mean, and the number of nights the star was observed in that filter. The estimated error is the larger of (1) the standard deviation of the mean, or (2)  $\sqrt{1/\sum(1/\sigma_{\text{night}}^2)}$ . Individual night’s magnitudes have been omitted if they deviated by more than  $3\sigma$  (or typically  $> 0^m.03$ ) from the mean, as defined by the value of  $\sigma$  after the omission. As the MKO filter set has been widely adopted because of its design advantages, and differs significantly from most earlier filter sets, including the UKIRT filters used by Hawarden et al (2001), we recommend that the present results are used instead of those of Hawarden et al., despite the latter’s superior internal accuracy (0<sup>m</sup>.005 cf. 0<sup>m</sup>.011).

The average number of nights each star was observed during this programme is 4. One LCO standard star, GSPC S705-D, appears to be variable, as 4–5 measurements produced standard deviations of 3–6% across *J*, *H* and *K*. Persson et al. (1998), however, found a small 1% deviation over their four measurements of this star. The UKIRT standard FS 144 (Ser-EC84) has been reported as possibly variable at the 5% level, and possibly binary (N. Cross, M. Connelley, private communications), although our three measurements agree to 3% at *J* and 1% at *H* and *K*. There are two UKIRT standards for which the magnitudes presented here are fainter than the UKIRT-system values (Hawarden et al. 2001; Casali & Hawarden 1992) by  $\sim 0^m.1$  :

**Table 3.** Measured MKO *JHK* magnitudes.

UKIRT FS No.	Name	mag	$J_{MKO}$ Std.Dev.	Nts.	mag	$H_{MKO}$ Std.Dev.	Nts.	mag	$K_{MKO}$ Std.Dev.	Nts.	Note
101	CMC 400101	10.540	0.005	4	10.405	0.012	4	10.366	0.016	5	1
...	BRI B0021-0214	11.754	0.007	4	11.082	0.011	6	10.500	0.008	6	
102	GSPC P525-E	11.583	0.013	3	11.273	0.008	3	11.200	0.012	3	
1	G158-100	13.427	0.006	3	13.059	0.011	3	12.984	0.019	3	
103	GSPC P241-G	12.342	0.011	4	11.840	0.008	6	11.724	0.012	3	
2	SA92-342	10.699	0.005	4	10.495	0.009	4	10.470	0.009	4	1
...	GSPC S754-C	11.008	0.009	4	10.721	0.008	4	10.669	0.007	4	
3	Feige 11	12.649	0.009	5	12.739	0.011	4	12.840	0.012	4	
104	GSPC P194-R	10.503	0.008	6	10.414	0.013	5	10.395	0.013	4	1
105	GSPC P527-F	11.526	0.012	5	11.070	0.010	5	10.961	0.007	5	
106	GSPC P152-F	12.466	0.009	3	11.877	0.013	3	11.752	0.010	3	
107	CMC 600954	10.466	0.006	4	10.256	0.011	5	10.224	0.010	4	1
5	Feige 16	12.359	0.017	2	12.336	0.011	2	12.349	0.024	3	
4	SA 93-317	10.538	0.011	5	10.304	0.013	5	10.266	0.010	5	1
6	Feige 22	13.271	0.009	4	13.321	0.004	4	13.404	0.009	3	
...	GSPC P530-D	11.267	0.008	2	10.936	0.007	3	10.878	0.017	3	
7	SA 94-242	11.076	0.010	3	10.961	0.009	3	10.933	0.006	4	
108	CMC 502032	10.056	0.014	3	9.765	0.007	4	9.713	0.011	4	1
...	TVLM 832-38078	11.755	0.013	4	11.221	0.011	5	10.844	0.012	4	
109	LHS 169	11.435	0.015	4	10.983	0.011	4	10.813	0.010	4	
...	GSPC P247-U	11.907	0.009	4	11.606	0.007	3	11.508	0.013	4	
110	GSPC P533-d	11.703	0.011	4	11.406	0.004	4	11.321	0.007	4	
111	CMC 601790	10.618	0.013	4	10.361	0.004	3	10.275	0.016	4	1
112	GSPC S618-D	11.182	0.010	3	10.919	0.019	3	10.855	0.008	2	
10	GD 50	14.802	0.017	5	14.878	0.013	6	14.990	0.015	4	
113	GSPC P117-F	12.915	0.009	3	12.559	0.010	2	12.443	0.010	3	
114	Melotte 25 LH 214	14.373	0.009	4	13.876	0.010	3	13.434	0.008	2	
115	B216-b5	12.501	0.006	3	10.976	0.010	3	10.073	0.013	4	2
116	B216-b7	12.775	0.008	3	11.532	0.004	4	10.928	0.007	4	3
117	B216-b9	11.495	0.006	3	10.560	0.008	4	10.045	0.006	4	2
11	SA 96-83	11.329	0.005	3	11.264	0.013	3	11.241	0.008	3	
119	HD 289907	9.857	0.007	3	9.818	0.010	3	9.810	0.010	3	1
...	GSPC S840-F	11.365	0.016	3	11.099	0.013	3	11.019	0.009	3	
12	GD 71	13.710	0.009	4	13.805	0.018	4	13.899	0.011	3	
13	SA 97-249	10.471	0.009	4	10.176	0.007	4	10.126	0.009	4	1
120	LHS 216	11.299	0.015	3	10.855	0.011	4	10.603	0.011	4	
...	GSPC S842-E	11.660	0.020	3	11.327	0.013	3	11.233	0.014	3	
...	SA 98-653	9.428	0.014	5	9.422	0.016	5	9.443	0.010	4	1
121	GSPC S772-G	11.984	0.015	3	11.436	0.007	3	11.307	0.014	3	
122	GSPC P161-D	11.668	0.008	4	11.393	0.006	4	11.347	0.005	4	
14	Rubin 149A	14.128	0.006	4	14.164	0.017	5	14.214	0.016	4	
...	Rubin 149D	11.444	0.007	3	11.438	0.010	3	11.459	0.010	3	
...	GSPC P309-U	11.841	0.012	5	11.507	0.010	4	11.449	0.007	5	
...	GSPC S495-E	11.483	0.014	3	11.031	0.014	3	10.939	0.009	2	
...	GSPC P545-C	11.841	0.018	5	11.585	0.010	4	11.549	0.010	5	
...	LHS 2026	11.990	0.010	3	11.482	0.005	3	11.075	0.014	3	
...	GSPC S705-D	12.353	0.055	5	12.047	0.042	5	12.027	0.048	5	4
15	M67-I-48	12.722	0.008	4	12.423	0.014	5	12.359	0.013	4	
123	GSPC P486-R	10.126	0.012	4	10.158	0.010	4	10.203	0.007	4	1
16	M67-IV-8	12.968	0.014	5	12.702	0.009	5	12.650	0.015	6	
17	M67-IV-2	12.668	0.017	3	12.363	0.010	4	12.290	0.011	4	
124	LHS 254	11.467	0.018	5	11.085	0.007	4	10.727	0.009	3	
125	GSPC P259-C	10.797	0.006	4	10.423	0.011	4	10.355	0.007	4	1
126	GSPC P487-F	12.304	0.011	3	11.772	0.007	3	11.636	0.010	3	
...	GSPC S852-C	11.288	0.019	3	11.004	0.019	3	10.960	0.009	2	
...	GSPC S708-D	11.034	0.010	4	10.736	0.010	4	10.671	0.013	4	
127	GSPC P212-C	11.969	0.007	4	11.727	0.008	5	11.685	0.011	5	
19	G 162-66	13.625	0.015	6	13.691	0.012	7	13.789	0.017	6	
...	GSPC P550-C	12.293	0.014	3	12.083	0.004	3	12.052	0.008	3	
128	LHS 2347	12.985	0.008	3	12.421	0.005	3	12.046	0.017	3	
20	G 163-50	13.427	0.010	4	13.457	0.005	5	13.509	0.006	3	

**Table 3** – *continued*

UKIRT FS No.	Name	mag	$J_{MKO}$ Std.Dev.	Nts.	mag	$H_{MKO}$ Std.Dev.	Nts.	mag	$K_{MKO}$ Std.Dev.	Nts.	Note
129	LHS 2397aAB	11.792	0.005	5	11.173	0.010	5	10.639	0.009	5	
130	GSPC P264-F	12.980	0.008	2	12.402	0.005	3	12.262	0.011	3	
21	GD 140	13.021	0.007	3	13.075	0.011	3	13.167	0.017	3	
131	GSPC P266-C	11.617	0.009	3	11.362	0.010	3	11.324	0.012	4	
132	GSPC S860-D	12.159	0.012	4	11.879	0.015	4	11.835	0.012	4	
33	GD 153	14.085	0.007	3	14.165	0.010	3	14.296	0.011	2	
133	GSPC P172-E	12.330	0.011	3	11.971	0.006	3	11.909	0.008	3	
...	GSPC S791-C	11.605	0.011	3	11.283	0.014	3	11.227	0.015	4	
23	M3-193	12.990	0.006	3	12.488	0.004	3	12.397	0.009	3	
...	GSPC P133-C	11.113	0.024	4	10.876	0.006	4	10.832	0.009	5	
...	GSPC P499-E	11.893	0.008	3	11.560	0.031	3	11.528	0.008	2	
134	LHS 2924	11.885	0.013	4	11.251	0.010	5	10.721	0.013	5	
135	GSPC S867-V	11.965	0.010	2	11.669	0.007	3	11.604	0.007	3	
...	GSPC P272-D	11.601	0.008	4	11.267	0.011	4	11.212	0.008	4	
136	GSPC S868-G	12.531	0.012	4	12.014	0.009	5	11.893	0.012	5	
...	TVLM 868-53850	11.517	0.009	3	10.988	0.010	3	10.617	0.014	3	
...	TVLM 868-110639	12.530	0.020	4	11.875	0.009	4	11.306	0.015	2	
...	GSPC S870-T	10.862	0.005	3	10.667	0.012	3	10.632	0.012	3	5
...	GSPC P177-D	12.212	0.024	4	11.920	0.006	4	11.865	0.010	3	
137	GSPC P565-C	12.140	0.017	3	11.893	0.006	3	11.838	0.009	3	
138	GSPC P275-A	10.391	0.015	4	10.391	0.014	4	10.416	0.008	3	1
...	GSPC P330-E	11.772	0.017	5	11.455	0.017	5	11.419	0.011	4	
139	GSPC P137-F	12.671	0.023	5	12.228	0.015	5	12.126	0.010	5	
27	M13-A14	13.470	0.011	4	13.199	0.005	3	13.135	0.008	4	
140	GSPC S587-T	10.775	0.014	4	10.430	0.021	4	10.369	0.008	3	1
...	GSPC P138-C	11.327	0.027	2	11.124	0.007	2	11.098	0.019	3	
141	P489-D	11.152	0.015	3	10.853	0.009	3	10.785	0.011	3	
35	GSC 00441-01200	12.188	0.015	5	11.835	0.010	5	11.741	0.010	5	
143	Ser-EC68	16.495	0.030	3	14.269	0.010	2	12.923	0.011	3	
144	Ser-EC84	14.997	0.030	3	12.555	0.013	3	11.009	0.012	3	4
...	GSPC P182-E	12.081	0.006	4	11.779	0.013	3	11.713	0.011	3	
...	LDN 547	11.753	0.013	4	9.890	0.010	3	8.889	0.005	4	6
146	GSPC P280-U	10.708	0.008	4	10.209	0.006	4	10.120	0.012	4	1
147	GSPC P230-A	9.868	0.011	4	9.839	0.004	5	9.834	0.009	5	1
...	GSPC S808-C	10.925	0.013	3	10.628	0.014	3	10.543	0.009	3	5
148	GSPC S810-A	9.437	0.010	5	9.423	0.008	5	9.438	0.005	5	1
149	GSPC P338-C	10.073	0.012	3	10.061	0.018	5	10.061	0.015	5	1
150	CMC 513807	10.133	0.006	3	9.985	0.007	3	9.941	0.011	3	1
...	GSPC S813-D	11.434	0.014	4	11.118	0.009	4	11.053	0.012	4	
34	EG 141	12.883	0.009	4	12.930	0.013	4	13.000	0.016	2	
...	GSPC P576-F	12.215	0.011	3	11.924	0.007	3	11.854	0.015	3	
151	GSPC P340-H	12.211	0.014	3	11.946	0.008	3	11.865	0.014	3	
29	G 93-48	13.215	0.012	4	13.255	0.010	4	13.330	0.008	4	
...	BRI B2202-1119	11.595	0.007	3	11.085	0.013	4	10.708	0.010	3	
152	GSPC P460-E	11.648	0.013	4	11.130	0.009	4	11.048	0.007	4	
30	SA 114-750	11.936	0.005	3	11.975	0.014	4	12.013	0.012	4	
153	S820-E	11.603	0.013	4	11.029	0.012	4	10.890	0.009	4	
31	GD 246	13.845	0.017	3	13.961	0.009	4	14.064	0.014	4	
32	Feige 108	13.570	0.007	3	13.663	0.010	3	13.746	0.008	2	4
154	GSPC S893-D	11.373	0.008	3	11.098	0.012	4	11.050	0.008	3	
...	GSPC S677-D	11.811	0.009	6	11.559	0.012	5	11.537	0.014	6	
...	GSPC P290-D	11.617	0.009	3	11.331	0.009	3	11.255	0.016	3	
...	PG 2331+055A	15.333	0.030	4	15.381	0.031	5	15.404	0.040	4	
155	CMC 516589	9.964	0.009	4	9.472	0.016	5	9.383	0.013	6	1

(1) *JHK* may be too bright by  $\lesssim 0^m.02$  due to non-linearity underestimate(2) *K* may be too bright by  $\lesssim 0^m.02$  due to non-linearity underestimate(3) May be variable at *J* by  $\sim 0^m.1$  over a period of years(4) May be variable at *JHK* by  $0^m.05$ – $0^m.10$  over a period of months to years(5) *J* may be too bright by  $\lesssim 0^m.02$  due to non-linearity underestimate(6) *HK* may be too bright by  $\lesssim 0^m.02$  due to non-linearity underestimate

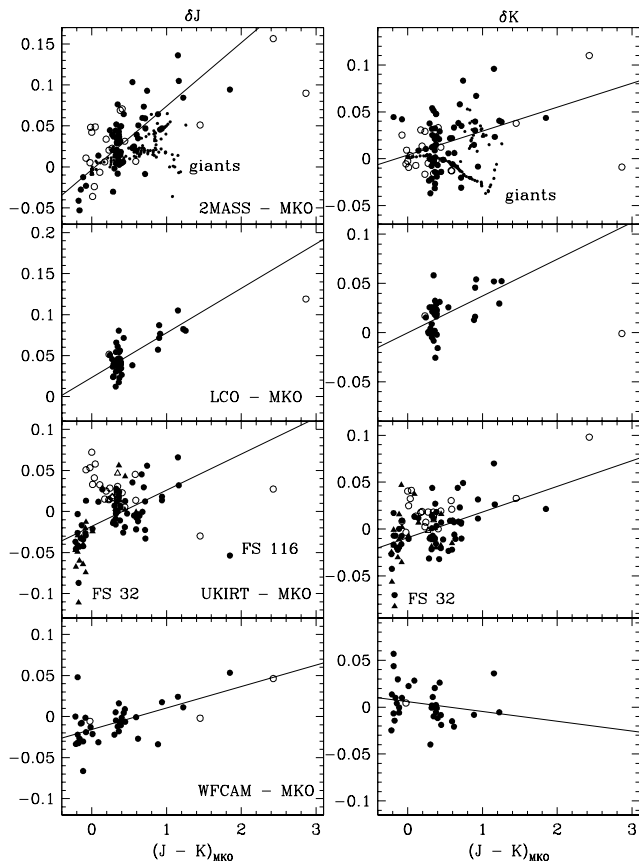


**Figure 2.** Differences between MKO-system  $J$  and  $K$  magnitudes and those of the 2MASS, LCO, UKIRT and WFCAM systems, as a function of  $J - K$  colour. Filled circles are stars with  $J > 11$  and  $K > 10.5$ , open are brighter stars that are not included in the linear fit, shown as a solid line. Triangles are data on the UKIRT system from Casali & Hawarden (1992). Small dots in the 2MASS plots in the top panels are synthetic results derived by Hewett et al. (2006) from spectra of dwarf and giant stars; red giants are brighter in 2MASS  $J$  and  $K_s$  than in MKO  $J$  and  $K$ , and their location is indicated by the “giants” label. FS 32 and FS 116 are identified in the UKIRT plots and are excluded from those fits. The MKO, WFCAM and 2MASS  $JHK$  and  $J$  are fainter than the UKIRT-system values for FS 32 and FS 116, respectively. The possible variables FS 144 and GSPC S705-D have been omitted from all plots.

FS 116 (B216-b7) and FS 32 (Feige 108, a subdwarf B star). The latter is significantly fainter at all  $JHK$ , the former at  $J$  only. The 2MASS and preliminary WFCAM values agree with the present results to  $< 0^m.05$ , suggesting that a change may have occurred between the epoch of the Casali & Hawarden and Hawarden et al. observations (1991 and 1994–1998, respectively) and that of the more recent 2MASS, MKO and WFCAM observations. We have indicated all four of these stars, GSPC S705-D, FS 144, FS 116 and FS32, as possibly variable in Table 3. An L dwarf companion has been found for the UKIRT standard FS 129 (M dwarf LHS 2397a, Freed, Close & Siegler (2003)), but this should not lead to detectable variability in the near-infrared.

Omitting S705-D, the average uncertainty of the mag-

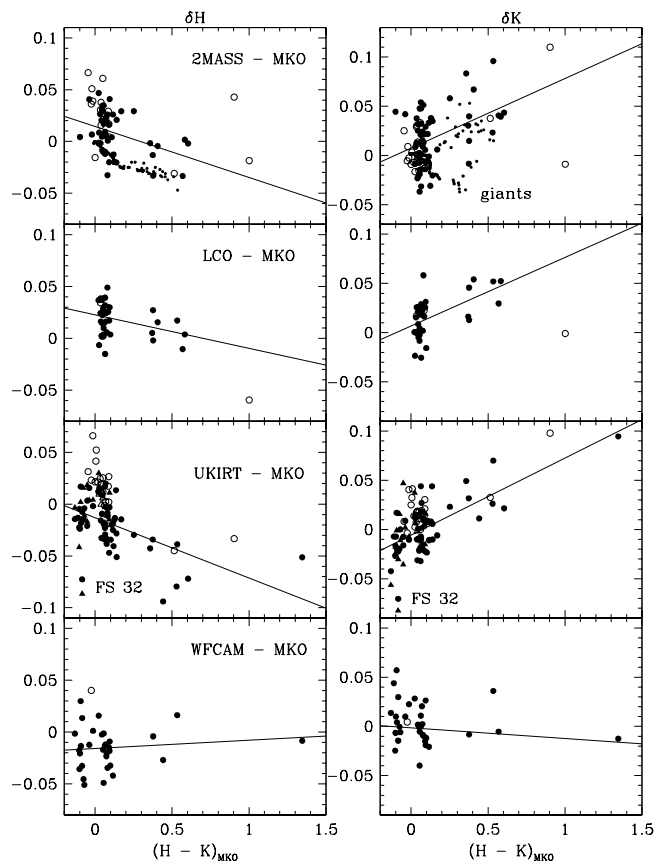


**Figure 3.** Differences between MKO-system  $H$  and  $K$  magnitudes and those of the 2MASS, LCO, UKIRT and WFCAM systems, as a function of  $H - K$  colour. Symbols and labels are as in Figure 2, except here filled circles are stars with  $H > 10.5$  and  $K > 10.5$ , open are brighter stars that are not included in the linear fit, shown as a solid line. FS 32 is indicated in the UKIRT plot, and excluded from the linear fits. The possible variables FS 144 and GSPC S705-D have been omitted from all plots.

nitudes listed in Table 3 is  $0^m.012$  at  $J$ , and  $0^m.011$  at  $H$  and  $K$ . These errors do not include systematic effects, and we explore these further below, through comparison with other published work.

## 6 COMPARISON WITH OTHER DATA

### 6.1 Datasets

In this section we compare our measured MKO  $JHK$  magnitudes with those measured for stars in common by: Hawarden et al. (2001) and the earlier UKIRT-system measurements by Casali & Hawarden (1992); Hunt et al. (1998) using the ARNICA camera with similar filters to the UKIRT-system set; the LCO (NICMOS) system from Persson et al. (1998); the 2MASS atlas; and preliminary MKO-system data from UKIRT’s Wide Field Camera, WFCAM. As we are looking for small effects, for the purpose of these comparisons we restrict each dataset to values with uncertainty  $< 0^m.025$ .

**Table 4.** Colour Transformations.

$\delta$ mag	constant A	error A	slope B	error B	colour
$J_{2\text{MASS}} - J_{\text{MKO}}$	-0.004	0.006	+0.078	0.010	$J - K_{\text{MKO}}$
$K_{2\text{MASS}} - K_{\text{MKO}}$	+0.004	0.007	+0.026	0.011	$J - K_{\text{MKO}}$
$K_{2\text{MASS}} - K_{\text{MKO}}$	+0.008	0.004	+0.071	0.020	$H - K_{\text{MKO}}$
$H_{2\text{MASS}} - H_{\text{MKO}}$	+0.014	0.004	-0.049	0.018	$H - K_{\text{MKO}}$
$J_{\text{MKO}} - J_{2\text{MASS}}$	+0.001	0.006	-0.069	0.010	$J - K_{2\text{MASS}}$
$K_{\text{MKO}} - K_{2\text{MASS}}$	-0.003	0.008	-0.025	0.012	$J - K_{2\text{MASS}}$
$K_{\text{MKO}} - K_{2\text{MASS}}$	-0.006	0.006	-0.065	0.030	$H - K_{2\text{MASS}}$
$H_{\text{MKO}} - H_{2\text{MASS}}$	-0.014	0.004	+0.049	0.022	$H - K_{2\text{MASS}}$
$J_{\text{LCO}} - J_{\text{MKO}}$	+0.023	0.005	+0.055	0.009	$J - K_{\text{MKO}}$
$K_{\text{LCO}} - K_{\text{MKO}}$	-0.001	0.006	+0.037	0.010	$J - K_{\text{MKO}}$
$K_{\text{LCO}} - K_{\text{MKO}}$	+0.007	0.004	+0.070	0.018	$H - K_{\text{MKO}}$
$H_{\text{LCO}} - H_{\text{MKO}}$	+0.023	0.003	-0.032	0.015	$H - K_{\text{MKO}}$
$J_{\text{MKO}} - J_{\text{LCO}}$	-0.019	0.005	-0.058	0.008	$J - K_{\text{LCO}}$
$K_{\text{MKO}} - K_{\text{LCO}}$	0.003	0.006	-0.038	0.010	$J - K_{\text{LCO}}$
$K_{\text{MKO}} - K_{\text{LCO}}$	-0.007	0.004	-0.071	0.020	$H - K_{\text{LCO}}$
$H_{\text{MKO}} - H_{\text{LCO}}$	-0.023	0.003	+0.034	0.017	$H - K_{\text{LCO}}$
$J_{\text{UKT}} - J_{\text{MKO}}$	-0.018	0.004	+0.044	0.008	$J - K_{\text{MKO}}$
$K_{\text{UKT}} - K_{\text{MKO}}$	-0.010	0.004	+0.027	0.006	$J - K_{\text{MKO}}$
$K_{\text{UKT}} - K_{\text{MKO}}$	-0.006	0.003	+0.078	0.010	$H - K_{\text{MKO}}$
$H_{\text{UKT}} - H_{\text{MKO}}$	-0.013	0.003	-0.058	0.011	$H - K_{\text{MKO}}$
$J_{\text{MKO}} - J_{\text{UKIRT}}$	+0.017	0.004	-0.044	0.007	$J - K_{\text{UKIRT}}$
$K_{\text{MKO}} - K_{\text{UKIRT}}$	+0.009	0.004	-0.027	0.006	$J - K_{\text{UKIRT}}$
$K_{\text{MKO}} - K_{\text{UKIRT}}$	+0.005	0.003	-0.089	0.012	$H - K_{\text{UKIRT}}$
$H_{\text{MKO}} - H_{\text{UKIRT}}$	+0.014	0.003	+0.064	0.013	$H - K_{\text{UKIRT}}$

## 6.2 Colour Transformations

Colour transformations must be derived to correct for the different filter profiles (see Figure 1). To do this, we plotted the differences between the MKO data presented here and the six datasets listed above (as  $\delta J$ ,  $\delta H$  and  $\delta K$ ), as a function of the MKO colours  $J - K$  and  $H - K$ . In §6.3 we show that there are indications of non-linearity effects for stars brighter than 11th magnitude at  $J$  and 10<sup>m</sup>.5 at  $H$  and  $K$ ; hence to derive the colour transformations we used only stars fainter than these limits.

Figure 2 shows  $\delta J$  and  $\delta K$  as a function of  $J - K$ , and Figure 3 shows  $\delta H$  and  $\delta K$  as a function of  $H - K$ . The Hunt et al. (1998) data span a small range in colour and are not shown in the figures. The Casali & Hawarden (1992) UKIRT dataset did not span a large colour range, and the existing data showed close agreement with the later Hawarden et al. (2001) data, as expected due to their use of the same filters. These two UKIRT-system datasets are shown together in one row in Figures 2 and 3. We adopt the same colour transformation for the two datasets, derived from the more accurate Hawarden et al. (2001) results.

In the 2MASS rows in Figures 2 and 3 we also show differences derived from synthetic magnitudes by Hewett et al. (2006). Hewett et al. determined  $JHK$  MKO- and 2MASS-system magnitudes from the Bruzual-Persson-Gunn-Stryker Spectral Atlas<sup>2</sup> and additional M dwarf spectra taken from the literature, for a study of the UKIDSS photometric system. The authors find that colour transformations between 2MASS and MKO are a function of stellar luminosity class, and this can also be seen in Figures 2 and 3. Red dwarfs and giants with the same  $J - K$  or  $H - K$  colour can differ in  $J$  or

$K$  by 0<sup>m</sup>.05, between the two systems. Examining the spectra of an M2V and an M3III star, both with  $H - K \sim 0.3$ , shows that the wider 2MASS  $J$  filter detects the water bands in the dwarf spectrum, and the redder MKO  $K$  filter is sensitive to the strong CO absorption in the red giant (see the filter bandpasses in Figure 1). The  $H$  filters sample similar spectral features, and the offset seen in  $\delta H$  in Figure 3 is simply a difference in zeropoint. However, it must be borne in mind that for astronomical objects with very structured spectral energy distributions, such as T dwarfs, magnitudes can be system-dependent at the several-tenths of a magnitude level (Stephens & Leggett 2004).

WFCAM on UKIRT contains MKO-system filters and therefore there should be no colour dependency between the WFCAM and UFTI magnitudes presented here. Figure 3 shows that  $\delta H$  and  $\delta K$  are consistent with no colour term, but there is a suggestion of a colour dependency at  $J$  in Figure 2. The relationship is heavily weighted by the reddest star and the slope is probably spurious. This will be investigated further as more WFCAM data are obtained and the WFCAM photometric response better understood.

Table 4 gives colour transformations between MKO and the 2MASS, LCO and UKIRT systems, where

$$\delta mag = A \pm error_A + (B \pm error_B * colour)$$

Differences in colours can be calculated from the differences in magnitudes. The LCO transformation should be treated cautiously as it is not well determined (see Figures 2 and 3). Also, as described above, a single transformation cannot describe the 2MASS to MKO relationship to better than ~5% due to the intrinsic dependency on luminosity class.

All the photometric systems considered here are Vega-based, where Vega is defined to have zero magnitude in  $J$ ,  $H$  and  $K$ . The MKO, UKIRT, WFCAM and LCO systems

<sup>2</sup> <http://www.stsci.edu/hst/observatory/cdbs/bpgs.html>

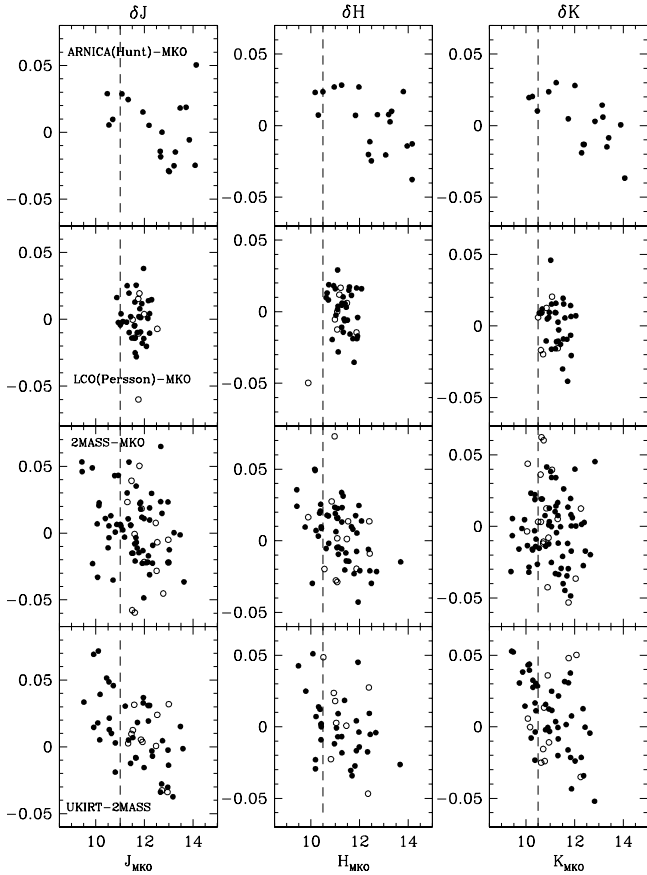


**Figure 4.** Differences between MKO-system  $J$ ,  $H$  and  $K$  magnitudes and those of the ARNICA, LCO and 2MASS systems, after transformation to MKO, as a function of  $JHK_{\text{MKO}}$  brightness. A comparison between UKIRT (Hawarden et al. 2001) and 2MASS is also shown, where the 2MASS data has been transformed to the UKIRT system, and the results plotted against UKIRT  $JHK$ . Filled circles are stars bluer than  $J - K = 0.7$ , which have more accurate colour transformations between systems, and open circles are redder stars. The dashed line separates stars brighter and fainter than  $J = 11$  and  $H, K = 10.5$ , see discussion in text. The possibly variable stars FS 144, FS 32 and GSPC S705-D have been omitted from all plots, and FS 116 is excluded in the UKIRT  $J$  plot.

are linked to Elias et al. (1982), who adopt Vega to be zero in all bands. 2MASS used LCO and UKIRT calibrators to calibrate their fields. Thus, the linear fits shown in Figures 2 and 3 should go through (0,0). Table 4 (columns 2 and 3) shows that LCO  $J$  and  $H$  have a small  $\sim 0^{\text{m}}02$  offset, significant at the 4–7  $\sigma$  level (as also seen in the UKIRT comparison by Hawarden et al. (2001)); 2MASS  $H$  and UKIRT  $JHK$  have smaller  $0^{\text{m}}010$ – $0^{\text{m}}015$  offsets significant at the 3  $\sigma$  level. These may reflect small drifts introduced into the systems’ zeropoints with each step away from the initial, bright, Elias et al. (1982) reference standards (for example the MKO dataset presented here is linked to the UKIRT Hawarden et al. (2001) dataset which is linked to the Casali & Hawarden (1992) dataset, which used Elias et al. (1982) standards).

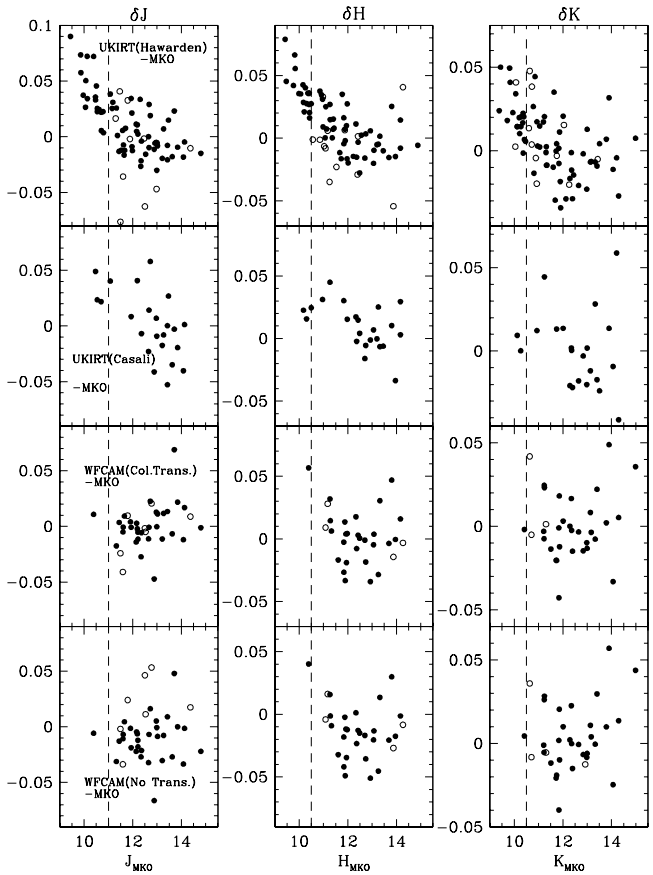


**Figure 5.** Differences between MKO-system  $J$ ,  $H$  and  $K$  magnitudes and those of the UKIRT and WFCAM systems, as a function of  $JHK_{\text{MKO}}$  brightness. The UKIRT data have been transformed to the MKO system, the WFCAM data are shown both with and without a colour transformation. Symbols are as in Figure 4. UKIRT(Casali) is Casali & Hawarden (1992) data, and UKIRT(Hawarden) is Hawarden et al. (2001) data. The possibly variable stars FS 144, FS 32 and GSPC S705-D have been omitted from all plots, and FS 116 is excluded in the UKIRT  $J$  plots.

### 6.3 Data Comparison and Non-Linearity Effects

#### 6.3.1 $\delta\text{mag}$ as a function of brightness

Having derived the colour transformations between systems, we can now compare our results with other published values. To do this, we have applied the colour transformations derived above to each dataset, and calculated the difference in magnitudes. Due to the fact that our monotonic transformation does not take luminosity class into account, and hence may introduce an error for redder stars, the primary comparison sample consists of stars with  $J - K < 0.7$ , as well as uncertainties in magnitudes  $< 0^{\text{m}}025$ . Red and blue stars are differentiated by symbols in Figures 4 and 5, which plot  $\delta\text{mag}$  as a function of  $\text{mag}_{\text{MKO}}$  for the ARNICA, LCO, 2MASS, UKIRT and WFCAM samples. The WFCAM comparisons are plotted both with the colour terms suggested in Figures 2 and 3 applied, and with no colour term applied.

The clearest trends in Figures 4 and 5 are seen in the UKIRT – 2MASS and UKIRT – MKO comparisons. The

UKIRT – MKO correlation is such that brighter stars are fainter in the UKIRT system or brighter in the MKO system. Due to the opposite senses of the non-linearity behaviours of the cameras used for the UKIRT and MKO datasets, this could point to a problem with either dataset, or both. In fact, the unusual UFTI response is such that it exaggerates any non-linearity in any of the comparison datasets, if any non-linearity remains in the UFTI data. The comparisons with 2MASS for the UKIRT Hawarden et al. data and the MKO data presented here (bottom two rows in Figure 4) suggest a correlation with the UKIRT data, and a less significant correlation with the MKO data (linear regression t-statistics imply the slopes are significant at the 4, 2 and 5  $\sigma$  level at  $J$ ,  $H$  and  $K$  respectively for the UKIRT comparison, and 2, 4 and 0  $\sigma$  for the data presented here).

These observed trends spurred an investigation of non-linearity effects in the MKO, UKIRT, WFCAM and 2MASS datasets. Large scatter or small magnitude range in the samples considered here make the comparison to the Casali & Hawarden (1992); Hunt et al. (1998); Persson et al. (1998) data inconclusive.

### 6.3.2 Applied linearity corrections

The 2MASS data does not have a linearity correction applied as such, but all raw data are inspected and for any data with signal at the level of 1% deviation from linearity, the first read of the image was used as opposed to the two-read image (R. Cutri private communication). As the “Read2 - Read1” exposure saturation threshold is around  $K_s = 8.0$ , the  $K > 9$  stars studied here should be safely in the linear regime for the 2MASS data, given the option of using the first-read data only.

The linearity response of the WFCAM detectors appears to be flat to 1% over a large range in counts (Hodgkin, private communication). However stars 11th magnitude and brighter will have peak pixels approaching saturation, and aperture photometry on such stars will be too faint by  $\gtrsim 0^m02$ . No trends are seen with brightness for the WFCAM data shown in Figure 5, suggesting that, at least for this fainter subset of our sample, the WFCAM and MKO data are linear.

We re-reduced the UKIRT and MKO data, taken with the IRCAM and UFTI cameras respectively, exploring how changes in the linearity correction affect the data. Doubling the correction applied resulted in a  $\leq 0^m01$  change in the final result. This is due both to the small size of the correction, and also to our way of reducing both the IRCAM and UFTI data in a relative sense, deriving an average zero-point for each night’s set of stars. However problems with the linearity correction may still exist.

### 6.3.3 Errors in the applied linearity corrections

Persson et al. (1998) point out that it is easy to underestimate non-linearity effects for very bright stars, with short exposure times, when using double-read mode. Both reads of the pair may be further up the non-linear curve than realised.

We can estimate the size of this effect for the data presented here and by Hawarden et al. (2001) by assuming that

the correction to each individual read is the same as that derived experimentally for the double-read mode. If the exposure time is equal to the read time, then the first read will have counts  $\sim$ half those of the second read. In this case, for UFTI, if the second read is say 10000 DN, then applying the linearity correction to each read instead of the difference of the reads, leads to a signal difference of 6.1% for this pixel, where the true value is lower. If the exposure time is twice the read time, so that the first read is  $\sim$ one-third of the second, and the second read is 9000 DN, then the difference is 3.6% for that pixel. The same calculations for IRCAM also produce a  $\sim$ 4% effect, although here the true signal level is higher.

The effect on the aperture photometry is smaller than this; on a night with UKIRT’s typical  $0^{\prime\prime}.7$  seeing, around one-third of the total flux would arise from pixels with counts within a factor of two of the maximum. Hence a 1–2% effect is likely for stars observed with exposure times 1–2 $\times$  the read time, or 9th–11th magnitude stars for the MKO (UFTI) and UKIRT (IRCAM) samples, in average to good seeing, at  $J$ ,  $H$  and  $K$ . For stars fainter than 11th magnitude, the exposure time is  $\geq 3$ –5 $\times$  the read time, and the effect on the aperture photometry is calculated to be  $\leq 0.5\%$ . This means that the UKIRT to MKO comparisons in Figures 4 and 5 would show a  $\sim 0^m04$  effect for bright stars, and the 2MASS comparisons would show a  $0^m02$  effect (assuming the 2MASS data are linear), as is in fact seen.

The combination of exposure times and filters used for this work, and by Hawarden et al., led to counts on the standard star being larger at  $J$  than at  $H$  and  $K$ , for both datasets. Hence the error in the non-linearity correction is significant at fainter values of  $J$  than of  $H$  and  $K$ . Linear regression to the UKIRT – MKO plots shown in Figure 5 gives correlation coefficients and t-statistic values of 0.7 and 8, 0.7 and 9 and 0.5 and 5, for  $J$ ,  $H$  and  $K$ , respectively, where the entire sample is considered. Excluding stars with  $J < 11$  and  $H, K < 10.5$  reduces these to insignificant values of 0.4 and 2.5, 0.4 and 3 and 0.2 and 1.5.

Given the stronger correlation between the 2MASS and UKIRT values than between 2MASS and MKO (Figure 4), and the larger pixels in IRCAM than UFTI ( $0^{\prime\prime}.28$  cf.  $0^{\prime\prime}.09$ ), it’s likely that more of the non-linearity error lies in the earlier Hawarden et al. (2001) data than in the data presented here. In any case, the systematic effect on the data presented here is small:  $+0^m005 - +0^m020$  for the 25 stars with  $J < 11$  or  $H, K < 10.5$ . For the 90 fainter stars in the sample, the error is a factor of two, or more, less than the measurement error, and hence insignificant.

## 7 CONCLUSIONS

We have presented  $JHK$  magnitudes for 115 stars in the brightness range of 10–15th magnitude. The photometry is in the widely adopted MKO photometric system, which uses well-defined filters matched to the atmospheric windows. The internal accuracy is on average  $0^m011$ , with the stars being observed typically over 4 nights. The results presented here should be used in preference to those of Hawarden et al. (2001) if observations are being made in the MKO system, as the filters, and hence the photometric systems, are significantly different from the UKIRT system.

We present colour transformations between the MKO and the 2MASS, LCO and UKIRT photometric systems. However these transformations can be luminosity-class dependent at the 5% level for redder stars with strong absorption bands. For very accurate transformations between systems, the exact spectral type needs to be known and transformations calculated and applied as a function of type (or the stars should be observed in the required system).

We find that the difference between the *JHK* magnitudes presented here and those presented previously by Hawarden et al. (2001) shows a dependence on brightness. We explain this in terms of an under-estimate of the linearity correction for stars with  $J < 11$  and  $H,K < 10.5$ , such that the photometry presented here and by Hawarden et al. is affected by  $\lesssim 0^m.02$ . The effect is likely to be more significant in the results of Hawarden et al. than in the present results: this is supported by comparisons with 2MASS data.

There are 84 stars in the sample presented here that have  $11 < J < 15$  and  $10.5 < H,K < 15$ , are not suspected to be variable, and have magnitudes with an estimated error  $\leq 0^m.027$ ; 79 of these have an error of  $\leq 0^m.020$ . We recommend that these be adopted as primary standards for the MKO near-infrared (*JHK*) photometric system.

## ACKNOWLEDGMENTS

The United Kingdom Infrared Telescope is operated by the Joint Astronomy Centre on behalf of the U.K. Particle Physics and Astronomy Research Council. This work would not have been possible without the dedicated effort of all the UKIRT staff. We are grateful to A. Tokunaga for pursuing the MKO filters and to P. Hewett and S. Hodgkin for helpful discussion. This research has made use of the SIMBAD database, operated at CDS, Strasbourg, France. This research has also made use of the NASA/ IPAC Infrared Science Archive, which is operated by the Jet Propulsion Laboratory, California Institute of Technology, under contract with the National Aeronautics and Space Administration. This publication makes use of data products from the Two Micron All Sky Survey, which is a joint project of the University of Massachusetts and the Infrared Processing and Analysis Center/California Institute of Technology, funded by the National Aeronautics and Space Administration and the National Science Foundation. The Starlink Project was funded by the Particle Physics and Astronomy Research Council and managed by the Space Science and Technology Department of the Central Laboratory of the Research Councils. We are grateful to the referee whose comments led to a much improved manuscript.

## REFERENCES

Bakos, G. A., Sahu, K. C. & Németh, P., 2002, *Ap.J.Suppl.Ser.* 141, 187  
 Beckett, M. G., Mackay, C. D., McMahon, R. G., Parry, I. R., Ellis, R. S., Chan, S. J., Hoenig, M., 1998, *Proc. SPIE, Infrared Astronomical Instrumentation*, Ed. Fowler, A., 3354, 431  
 Bouchet, P., Schmider, F.X., Manfroid, J., 1991, *A&AS*, 91, 409

Cannon A. J. & Pickering E. C., 1989, *Henry Draper Catalogue and Extension 1*, *Harv. Ann.* 91-100 (1918-1924)  
 Carrasco, L., Garcia-Barreto, A., Recillas-Cruz, E., Cruz-Gonzalez, I., Serrano, A., 1991, *PASP*, 103, 987  
 Casali, M. M., Hawarden T. G., 1992, *The JCMT-UKIRT Newsletter*, 4, 35  
 Cavanagh, B., Hirst, P., Jenness, T., Economou, F., Currie, M. J., Todd, S. & Ryder, S. D., 2003, *Astronomical Data Analysis Software and Systems XII*, *ASP Conference Series*, Vol. 295, H. E. Payne, R. I. Jedrzejewski, and R. N. Hook, eds., 237  
 Cohen, M., Walker, R.G., Barlow, M.J., Deacon, J.R., 1992, *AJ*, 104,1650  
 Cohen, M., Wheaton, W.A., Megeath, S.T., 2003, *AJ*, 126, 1090  
 Colina, L. & Bohlin, R., 1997, *AJ*, 113, 1138  
 Drilling, J. S. & Landolt, A. U., 1979, *AJ*, 84, 783  
 Elias, J.H., Frogel, J.A., Matthews, K., Neugebauer, G., 1982, *AJ*, 87, 1029  
 Freed, M., Close, L. M., Siegler, N., 2003, *ApJ*, 584, 453  
 Fouqué, P., et al., 2000, *A&AS*, 141, 313  
 Gizis, J. E., 1997, *AJ*, 113, 806  
 Gizis, J. E., 2002, *Ap.J.*, 575, 484  
 Green R.F., Schmidt M., Liebert J., *The Palomar-Green Survey*, 1986, *Ap.J.Suppl.*, 61, 305  
 Greenstein, J. L. & Sargent, A. I., 1974, *Ap.J.Suppl.Ser.*, 28, 157  
 Guetter, H. H., Vrba, F.J., Henden, A.A., Luginbuhl, C.B., 2003, *AJ*, 125, 3344  
 Harrington, R. S. & Dahn, C. C., 1980, *AJ*, 85, 454  
 Hawarden, T.G., Leggett, S.K., Letawsky, M.B., Ballantyne, D.R., Casali, M.M., 2001, *MNRAS*, 325, 563  
 Heckmann O. & Diekvoss W., 1975, *AGK3: Star Catalogue of Positions and Proper Motions*, North of 2.5 degrees Declination  
 Hewett, P.C., Warren, S.J., Leggett, S.K., Hodgkin, S.T., 2006, *MNRAS*, 367, 454  
 The Tycho Reference Catalogue; Hog E., Kuzmin A., Bastian U., Fabricius C., Kuimov K., Lindegran L., Makarov V.V., Roeser S., 1998, *A&A*, 335, L65  
 Hunt, L.K., Mannucci, F., Testi, L., Migliorini, S., Stanga, R. M., Baffa, C., Lisi, F., Vanzi, L., 1998, *AJ*, 115, 2594  
 Kadla Z. I., 1966, *Izv. Glav. Astron. Obs.* 181, 93  
 Kirkpatrick, J. D., Henry, T. J. & Simons, D. A., 1995, *AJ*, 109, 797  
 Landolt, A.U., 1992, *AJ*, 104, 340  
 Lasker, B. M. et al., 1988, *The Guide Star Photometric Catalog*, *Ap.J.Suppl.Ser.*, 68, 1  
 Leggett, S. K., 1992, *Ap.J.Suppl.Ser.*, 82, 351  
 Leggett, S. K., Hawarden, T. G., Currie, M. J., Adamson, A. J., Carroll, T. C., Kerr, T. H., Kuhn, O. P., Seigar, M. S., Varricatt, W. P., Wold, T., 2003, *MNRAS*, 345, 144  
 McCook G. P. & Sion E. M., 1999, *Ap.J.Suppl.Ser.*, 121, 1  
 Perryman, M. A. C., et al., *The Hipparcos Catalogue*, 1997, *A&A*, 323, L49  
 Persson, S.E., Murphy, D.C., Krzeminski, W., Roth, M., Rieke, M. J., 1998, *AJ*, 116, 247  
 Pesch, P., 1967, *Ap.J.*, 148, 781  
 Price, S. D., Paxson, C., Engelke, C., Murdock, T.L., 2004, *AJ*, 128, 889  
 Puget, P., et al., 2004, *SPIE 5492*, 978, *Ground-based Instrumentation for Astronomy*, eds. A. Moorwood, M. Iye

- Reach, W.T., et al., 2005, PASP, 117, 978
- Reid , I. N. & Hawley, S. L., 1999, AJ, 117, 343
- Roche, P.F., Lucas, P.W., Mackay, C.D., Ettedgui-Atad, E., Hastings, P.R., Bridger, A., Rees, N.P., Leggett, S.K., Davis, C., Holmes, A.R., Handford, T., 2003, SPIE, 4841, 901, Instrument Design and Performance for Optical/IR Ground-Based Telescopes, eds. M. Iye and A.F. Moorwood
- Roeser, S. & Bastian, U., PPM North Star Catalogue, 1988, A&Ap.Suppl.Ser., 74, 449
- Salim S. & Gould, A., 2003, ApJ, 582, 1011
- Simons, D.A., Tokunaga, A., 2002, PASP, 114, 169
- Stephens, D.C., Leggett, S.K., 2004, PASP, 116, 9
- Stephenson, C. B., 1986, AJ, 91, 144
- Straizys, V. & Kalytis, R., 1981, AcA, 31, 93
- Tinney, C. G., 1993, Ap.J, 414, 279
- Tokunaga, A., Simons, D.A., Vacca, W.D., 2002, PASP, 114, 180
- Tokunaga, A., Vacca, W.D., 2005, PASP, 117, 421
- Tüg, H., White, N. M., Lockwood, G. W., 1977, A&A, 61, 679
- Tucholke, H. J., Scholz, R. D. & Brosche, P., 1994, A&Ap.Suppl.Ser., 104, 161
- Turnshek, D. A., Bohlin, R. C., Williamson, R. L., II, Lupie, O. L., Koornneef, J., & Morgan, D. H., 1990, AJ, 1243
- Vacca, W. D., Cushing, M. C., Rayner, J. T., 2004, PASP, 116, 352
- Zacharias N., Urban S. E., Zacharias M. I., Wycoff G. L., Hall D. M., Germain M. E., Holdenried E. R., Winter L., 2004, AJ, 127, 3043

This paper has been typeset from a  $\text{\TeX}$ / $\text{\LaTeX}$  file prepared by the author.